

Integrated Real-time Pneumatic Monitoring System with Triboelectric Linear Displacement Sensor

Zitang Yuan, Xiaosong Zhang, Qiang Gao, Zheng Wang, Tinghai Cheng and Zhong Lin Wang

Abstract—With the continuous development of mechanical automation field, its monitoring technology is also changing with each passing day. Pneumatic technology is one of the important ways to realize mechanical automation. Here, the integrated real-time pneumatic monitoring system (PMS) is proposed, which is composed of a triboelectric linear displacement sensor (TLDS) and a cylinder. The resolution of TLDS is 100 μm , which is composed of a slider and a stator. According to theory of freestanding triboelectric nanogenerator, the working principle of TLDS is explained. Therefore, the proposed PMS can realize displacement and speed monitoring of the full stroke of the cylinder. The experiment results show that the PMS enabled accurate monitoring of cylinder displacement and speed under different pressure conditions, and the mean error rate of PMS is less than 2%. In addition, to fulfill the actual demands of the pneumatic industry, the real-time hardware processing module is designed to realize real-time monitoring. Finally, the PMS still has stable monitoring performance after 6 h (about 4 km) continuous operation. This work successfully explored the application of triboelectric sensors in pneumatic system and reached the requirements of industrial applications.

Index Terms—pneumatic monitoring system (PMS), freestanding triboelectric nanogenerator, triboelectric linear displacement sensor (TLDS), mean error rate, real-time monitoring.

This work was supported in part by the National Key R&D Project from the Minister of Science and Technology (2016YFA0202701 and 2016YFA0202704), the Beijing Municipal Science and Technology Commission (Z171100002017017). (Corresponding author: Tinghai Cheng; Zhong Lin Wang.)

Z Yuan, X Zhang, Q Gao, Z Wang, T Cheng, and Z L Wang are with Beijing Institute of Nanoenergy and Nanosystems, Chinese Academy of Sciences, Beijing, 101400, China. (e-mail: 2202001101@stu.ccut.edu.cn; zhangxiao song@binn.cas.cn; 2201801004@stu.ccut.edu.cn; 2201801017@stu.ccut.edu.cn; chengtinghai@binn.cas.cn; zhong.wang@mse.gatech.edu)

Z Yuan, X Zhang, Q Gao, Z Wang, and T Cheng are with the Mechatronic Engineering Department, Changchun University of Technology, Changchun 130012, China.

T Cheng and Z L Wang are with CUSTech Institute of Technology, Wenzhou, Zhejiang, 325024, China.

Z L Wang is with School of Materials Science and Engineering, Georgia Institute of Technology, Atlanta, GA 30332-0245, United States.

I. INTRODUCTION

With the advent of the era of intelligent manufacturing, the application of mechanical automation technology has become increasingly widespread. Pneumatic technology is widely used in the automation industry because of its simple structure, low cost, and no pollution [1-5]. The cylinder is an important executive component of the pneumatic system. Its running status determines the efficiency of the pneumatic system. Therefore, detecting the piston position of the cylinder is an important task. At present, the sensor used for piston position detection is mainly the magnetic proximity switch. Moreover, some researchers have also done some research on detecting the position of the piston [6-10]. However, they are either point-positioned or the technical processes are complicated, or the degree of integration with the cylinder is low. Hence, it is imperative to need a new type sensor for monitoring the running status of cylinder, which has advantages of simple structure, convenient integration, and continuous monitoring.

Wang's group invented the triboelectric nanogenerator (TENG) based on the coupling of triboelectrification effect and electrostatic induction in 2012, which can effectively convert mechanical energy into electric signal [11-14]. Therefore, it has been widely used in micro/nano energy [15], [16], self-powered sensors [17], [18], large-scale blue energy [19], [20], and direct high voltage sources [21], [22]. Among them, the current triboelectric sensors mainly use some output parameter characteristics to achieve sensing detection, such as the change of voltage amplitude and the number of pulse signals. Therefore, various triboelectric sensors have been used by researchers in various fields, such as robot technology [23], [24], vehicle assisted driving [25], [26], flow/level measurement [27], [28], and motion monitoring [29], [30]. The triboelectric linear displacement sensor (TLDS) is used for motion monitoring and has the potential to detect running status of cylinder.

In recent years, several TLDSs have been developed for motion monitoring in different application scenarios. Zhang et al. reported a triboelectric sliding sensor for security monitoring and smart home systems [31]. Xie et al. studied a sweep-type triboelectric linear motion sensor for monitoring the position, velocity, and orientation of moving objects [32].

Wang et al. reported a self-powered dual-type signal triboelectric nanogenerator for real-time monitoring of autonomous vehicles [33]. Above research works are of great significance for the development of TLDS, but less of them have high resolution and back-end hardware modules, which limit their popularization and application to a great extent. Therefore, it is necessary to study a TLDS with higher resolution and back-end hardware modules.

Here, the integrated real-time pneumatic monitoring system (PMS) is composed of TLDS and cylinder, which realizes the monitoring of piston displacement and speed through pulse counting. The alternating current (AC) characteristics of the TENG are taken advantage of by the TLDS, which adopts a special phase-differential electrode designed to generate a special pulse signal with a resolution of 100 μm . From the theory of freestanding triboelectric nanogenerators, the process of charge transfer of TLDS is explained. The systematic experimental testing is carried out, taking the pressure range of 0.15-0.50 MPa as the experimental condition, the PMS can monitor the full stroke running status of cylinder in the positive and reverse motion with a mean error rate of less than 2%. In addition, a real-time hardware processing module successfully realized the real-time monitoring of the piston position, direction and speed. Finally, the durability experiment on PMS has verified its excellent monitoring function under continuous working conditions. This work will promote the application of triboelectric sensors in pneumatic industry.

II. STRUCTURE AND PRINCIPLE

Fig. 1(a) shows the schematic diagram of the assembly of PMS, it consists of rodless cylinder and TLDS. The basic structure of TLDS is shown in Fig. 1(b) (i) and (ii), it is composed of a slider and a stator. The slider consists of a Kapton film, a slider electrode, and a sponge rubber pad, and the stator consists of a stator electrode and an aluminum alloy plate. The above electrodes are all flexible printed circuit (FPC), which have the advantage of easy integration and adaptability to a variety of different working occasions. The slider is installed on the sidewall of the piston and then the stator is bolted to the side of the cylinder to align with the slider. The function of the sponge rubber pad is to make the slider electrode and the stator electrode contact more fully. The sensing unit of TLDS are slider electrode, Kapton film, and stator electrode. There are three-phase differential electrodes (A-Phase, B-Phase, C-Phase) which are misaligned on the stator electrode, and their arrangements are shown in enlarged drawing. They will generate three-phase signals with a specific phase difference, which can improve the resolution to 100 μm and distinguish the direction of the movement piston.

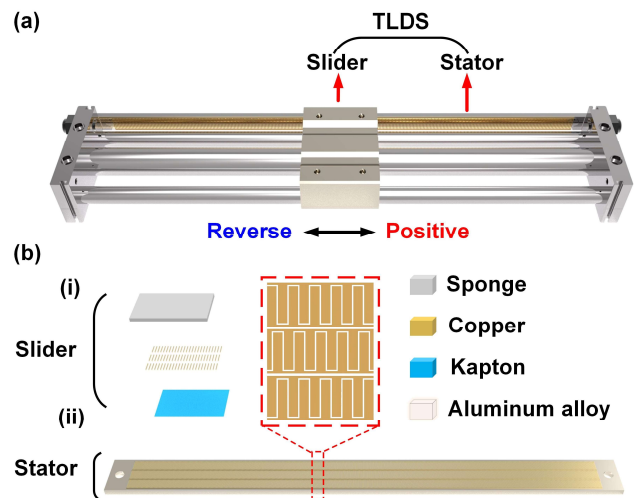


Fig. 1. (a) Schematic diagram of PMS. (b) Schematic structure of the TLDS.

The generation of the TLDS electrical signal depends on the contact sliding between the Kapton film and the copper electrode of the stator. The role of the copper electrode of the slider is to subdivide the Kapton film, which can improve the sensing accuracy. The signals generated by the three-phase differential electrode are divided into A-Phase, B-Phase, and C-Phase. Since the electrode shift between the three-phase differential electrodes is 1/6 period, the phase difference between the three-phase signals is $\pi/3$. TLDS works in freestanding mode whose core mechanism is the changeable capacitance ratio between Kapton film and copper electrode under the change of Kapton film position [34]. Fig. 2(a) illustrates the detailed working principle of the TLDS. Taking A-Phase as an example to illustrate the charge transfer process during TLDS operation, at the beginning, the Kapton film and copper-1 are perfectly aligned, and have equal amounts of positive and negative charges on the surface. At this moment, the TLDS is in electrostatic balance, the external circuit between copper-1 and copper-2 does not generate current. As the piston moves, the Kapton film gradually moves from copper-1 to copper-2. In this state, the generated potential difference makes the positive charges flow from copper-1 to copper-2. Thereby, a transient current can be formed on the external circuit. After the Kapton film reaches full overlap with the copper-2, it will reach an electrostatic equilibrium state again. As the piston continues to move positive, the positive charge will return to copper-1, creating an opposite current on the external circuit. Therefore, the relative movement between the slider and the stator will produce an AC output signal. Furthermore, to verify the electrical characteristics of the TLDS, the finite element simulation of the potential distributions in three different positions are performed. Furthermore, to verify the electrical characteristics of the TLDS, electrical simulations of the electrodes in three different positions were performed as shown in Fig. 2(b). The simulation results show the potential difference between the slider electrode and the stator electrode when the slider is in different positions.

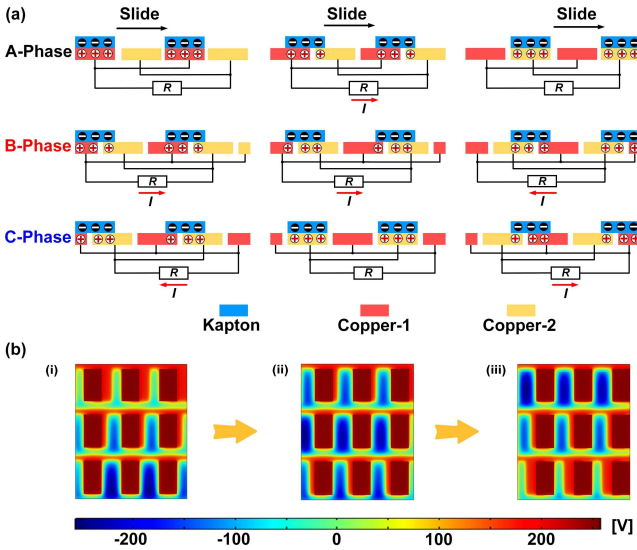


Fig. 2. (a) Schematic of the working principle of the different phase electrodes. (b) The finite element simulation of the potential distributions of the TLDS.

III. EXPERIMENTS AND DISCUSSIONS

To test the output performances, the PMS is manufactured and assembled, and an experimental system as shown in Fig. 3 is established, by which a series of experiments are performed. During the experiments, the rodless cylinder (CY1S, SMC, JPN) is the actuator of the pneumatic system and its stroke is fixed at 330 mm. The time delay (DH48S-S, OMRON, JPN) control of the electromagnetic reversing valve is realized by a timer. The accuracy of PMS is verified by the grating ruler (KA-300, SION, CN). Both the analog signal and the digital signal are input to the computer through the data acquisition card (USB-6210, NI, USA). The sensing test system is designed using the LabVIEW software platform to realize real-time data acquisition control and analysis. The structural size of prototype is shown in Table I.

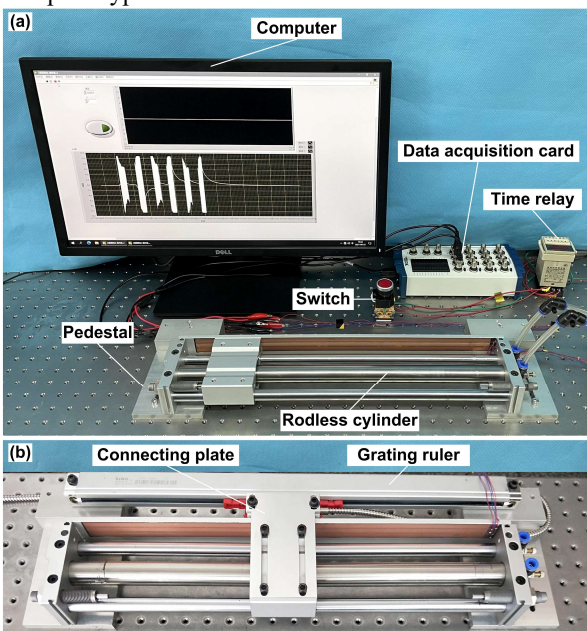


Fig. 3. (a) Experimental system for testing the performances of the prototype. (b) Experimental setup for comparison experiment.

TABLE I
GEOMETRICAL PARAMETERS OF THE PROTOTYPE.

Component	Geometrical parameters
Rodless cylinder	500×96×53 mm ³
Slider FPC	70×27 mm ² (thickness: 160 μm)
Stator FPC	465×27 mm ² (thickness: 160 μm)
One slider electrode	6.5×0.3 mm ² (thickness: 35 μm)
One stator electrode	6.5×0.2 mm ² (thickness: 35 μm)
Kapton film	70×27 mm ² (thickness: 55 μm)

Based on the analysis of the above principles, the PMS signal processing flow is designed. Fig. 4(a) shows that the signal waveform generated by TLDS is sine wave signal. Fig. 4(b) shows that the sine wave signal is converted into stable standard square signal through the hysteresis comparator and its phase and frequency characteristics remained unchanged. The direction of motion is determined by detecting the relationship between signal edges and levels. The specific implementation method is: select A-phase as the reference signal, when A-phase has a rising edge and B-phase is at a high level or vice versa, the signals of the other two phases lag behind A-phase, so they move forward, otherwise the direction of movement is opposite. The square wave is a standard transistor-transistor logic (TTL) level, which is conducive to the storage and processing of signals by the hardware. That is to realize the conversion of analog signals to digital signals. Fig. 4(c) shows that the digital signal is processed by MATLAB software to obtain the displacement and speed of the piston. The displacement is obtained by the pulse counting program in MATLAB software, and the speed is obtained by the differentiation of the displacement as shown in Fig. 4(c) (ii) and (iii).

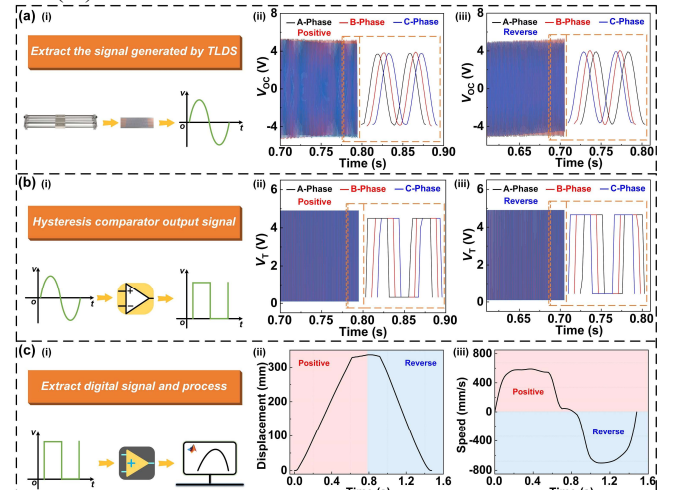


Fig. 4. (a) The analog signal generation and acquisition. (b) The digital signal is obtained by the comparator. (c) The acquired digital signal is processed by MATLAB (pressure=0.20 MPa).

Next, Fig. 5 illustrates the V_{OC} output characteristics of PMS at pressures of 0.15, 0.20, 0.30, 0.40, and 0.50 MPa, respectively. The voltage amplitude generated by PMS is basically stable when the cylinder moves in the positive and reverse directions, and its amplitude is about 10 V. The reason for the slightly different voltage amplitudes in different

directions and different air pressures is that the cylinder is not very smooth during the movement. The voltage characteristics obtained from the experimental results are consistent with the analyzed by the working principle described above. It guarantees the stability of PMS sensing, which provides a guarantee for the subsequent signal processing.

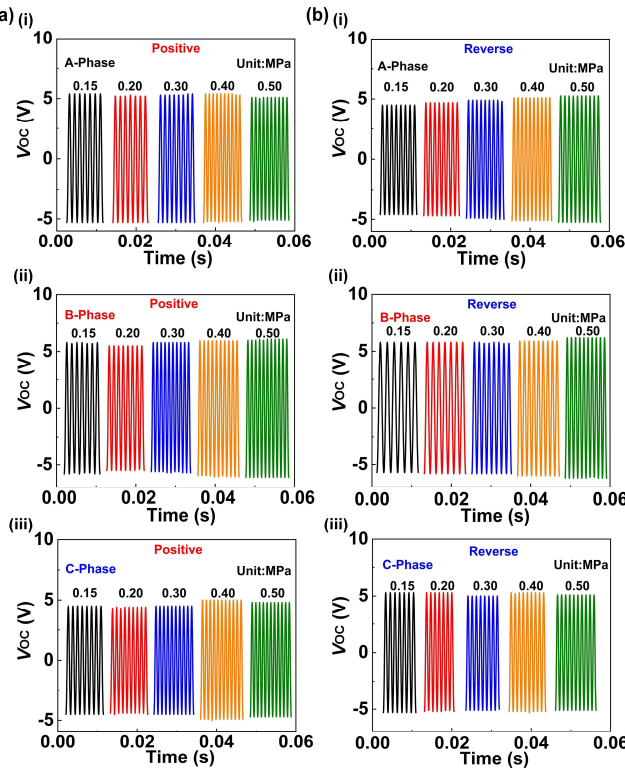


Fig. 5. (a) V_{OC} of PMS for positive cylinder motion at different pressures.
(b) V_{OC} of PMS for cylinder reverse motion at different pressures.

The comparison experiment is designed to verify the measurement accuracy of PMS. The two sets of data obtained are processed by MATLAB software and the displacement measured by PMS and grating ruler are obtained respectively. The displacement calculation equation is as follows:

$$S = nr \quad (1)$$

where S is the displacement measured by PMS, n is the number of voltage signals generated by the PMS, and r is the resolution of the PMS. As shown in Fig. 6, five different pressures of 0.15, 0.20, 0.30, 0.40, and 0.50 MPa are selected for experimental testing. The piston displacement curve obtained by the PMS measurement is basically consistent with the curve obtained by the grating ruler. Even if a small area in the displacement is selected to be enlarged, the measurement results of the two measurements still maintain a superior consistency. The violent shock of the cylinder when changing direction leads to errors in the test system, which can cause the start and end points of the measured displacement of the PMS and the grating scale to be slightly different.

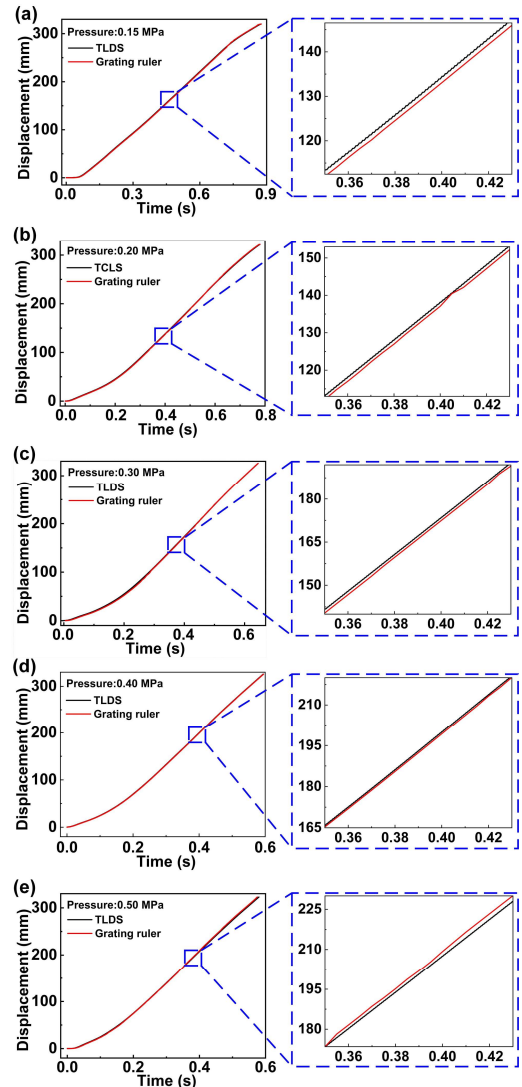


Fig. 6. Comparison experiment between PMS and grating ruler under different pressures, (a) pressure=0.15 MPa, (b) pressure=0.20 MPa, (c) pressure=0.30 MPa, (d) pressure=0.40 MPa, (e) pressure=0.50 MPa, (displacement=330 mm).

In addition, under the same pressure the piston movement time of cylinder is selected as 0.3, 0.4, 0.5, and 0.6 s, respectively. After data processing, four sets of displacement curves are obtained as shown in Fig. 7. It shows that the PMS enables the monitoring of the piston when it is in different positions.

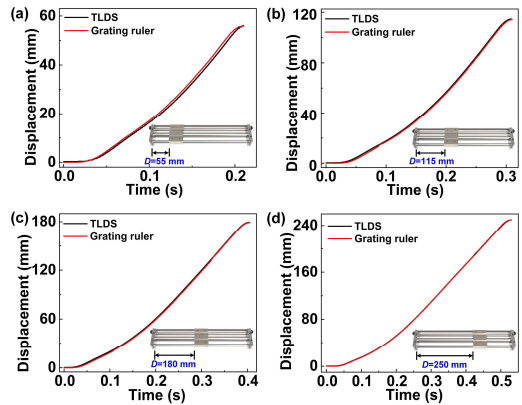


Fig. 7. Comparison experiment between PMS and grating ruler under piston different movement time (pressure=0.30 MPa).

The speed of the piston is obtained by differentiating the displacement measured by PMS. The speed equation of the piston is as follows:

$$v_c = \frac{ds}{dt} \quad (2)$$

where v_c is the speed of the piston, ds is the distance moved by the piston, and dt is the movement time of the piston. The speed information is shown in Fig. 8. When the piston is moving at full stroke, its speed increases as the pressure increases, as shown in Fig. 8(a). When the pressure is the same, the speed increases with the piston displacement as shown in Fig. 8(b), because the acceleration of the piston takes period of time.

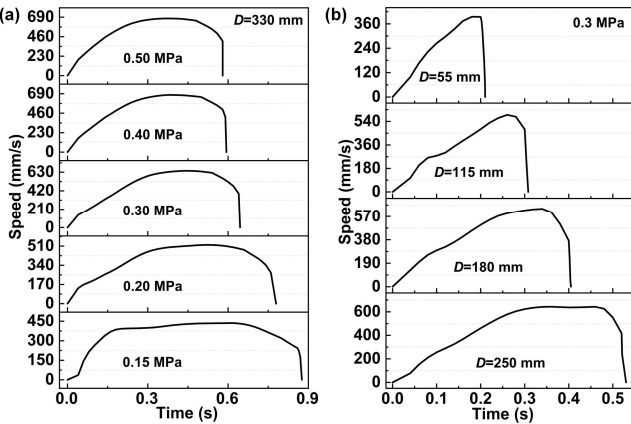


Fig. 8. (a) The speed of the piston at different pressures. (b) The speed of the piston in different movement time.

Next, the mean error rate of the PMS measurement displacement of the piston at different displacements is calculated. The mean error rate calculation equation of PMS is as follows:

$$\delta_i = \frac{|S_i - S_0|}{S_0} \times 100\% \quad (3)$$

$$\tilde{\delta}^{(j)} = \frac{1}{m} \sum_{i=1}^m \delta_i \quad (4)$$

$$\bar{\delta} = \frac{1}{n} \sum_{j=1}^n \tilde{\delta}^{(j)} \quad (5)$$

where δ_i is the error rate at different pressures, S_i is the displacement measured by PMS, S_0 is the displacement measured by grating ruler, $\tilde{\delta}^{(j)}$ is the mean error rate at different pressures ($m=5$), $\bar{\delta}$ is the mean error rate in multiple measurements ($n=3$). As shown in Fig. 9, it is concluded that the displacement error rate of PMS measured displacement is less than 2% compared with that of the grating ruler. And the error rate of PMS tends to decrease with the increase of piston displacement, due to the higher resolution of the grating ruler than the PMS. At the maximum displacement of the piston, the error rate is less than 0.3%. The above shows that the PMS can monitor the running status of the cylinder for the full stroke and has good accuracy.

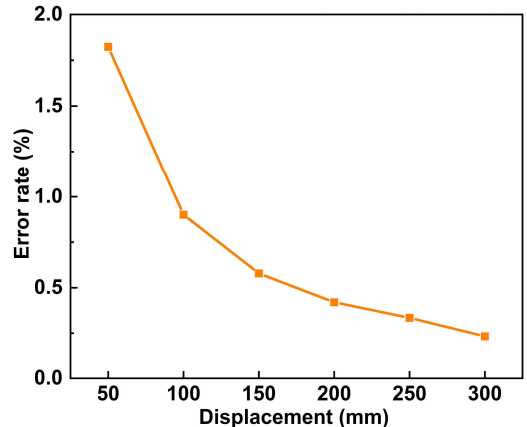


Fig. 9. The mean error rate of PMS at different displacement.

To the actual service condition of the pneumatic industry, a real-time hardware processing module is built. The sine wave signal generated by TLDS becomes square wave signal through a voltage comparison circuit as shown in Fig. 10(a). The generated square wave is input into the microprogrammed control unit (MCU) to obtain the displacement and speed through its counting program. Finally, these motion parameters are displayed in real-time through the display screen. The photo of the printed circuit board (PCB) is shown in Fig. 10(b) (i), which dimensions are 62 mm in length and 45 mm in width. The photo of the integrated hardware is shown in Fig. 10(b) (ii). The real-time hardware processing module is powered by 4 AAA batteries. The experimental results show that PMS can realize real-time monitoring of the position, speed and direction of piston. The PMS is capable of real-time display, integration and miniaturization to meet practical application conditions.

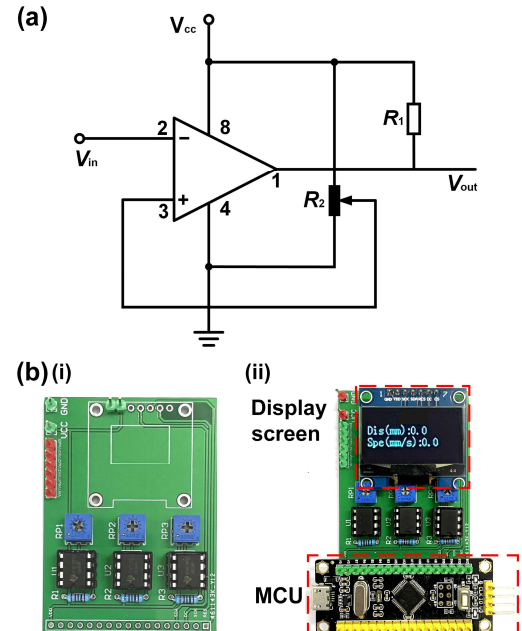


Fig. 10. (a) Circuit diagram of voltage comparator. (b) (i) The PCB of the voltage comparator circuit and (ii) real-time hardware processing module.

The durability test is designed to verify the reliability of PMS and select pressure is 0.20 MPa and the operation period

is 1.8 s as experimental condition. The experimental data of the A-phase signal in the three-phase signal is collected which is collected every 1 h as shown in Fig. 11. After the PMS runs continuously for 6 h, although the voltage amplitude decreases to a certain extent, the frequency during stable operation remains basically unchanged, which has no effect on its sensing accuracy. The signal obtained during this period still realizes a stable digital signal output. The above experiments show that PMS has fine repeatability and provides a guarantee for practical applications.

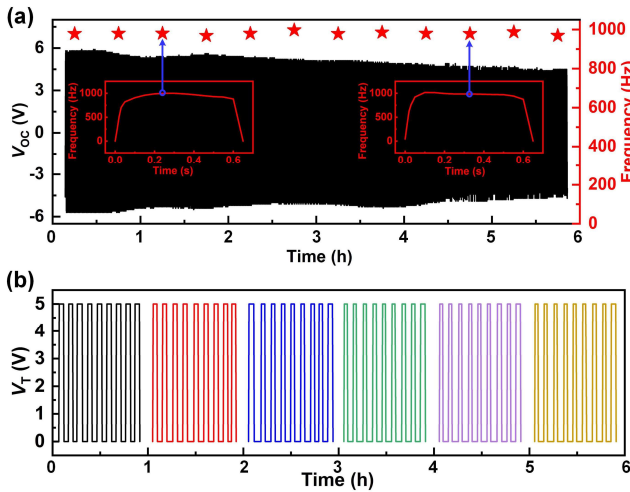


Fig. 11. (a) Original voltage signal amplitude and time-frequency diagram (A-Phase). (b) Digital signal diagram of different time periods (A-Phase).

IV. CONCLUSION

In summary, TLDS and cylinder form the PMS, which is used for cylinder running status monitoring. The TLDS is proposed by using the characteristics of pulse signals generated by TENG, it consists of a slider and a stator, and it has the resolution of 100 μ m. The TLDS adopts the three-phase differential electrodes for improving the resolution and distinguishing the direction. The working principle of TLDS is analyzed in detail. In the pressure range of 0.15–0.50 MPa, the PMS realizes the detection of the full-stroke bidirectional displacement and speed of the piston. To prove the measuring accuracy of PMS, a comparison experiment is carried out with the grating ruler and PMS. The result is that the mean error rate of PMS is less than 2%. Moreover, the real-time hardware processing module is designed which successfully realized real-time monitoring of piston displacement and speed. Finally, the output performance of PMS is relatively stable after 4 km of continuous operation, which proves its fine repeatability. The research proposes a new method for detecting the piston position of a cylinder and further promotes the application of triboelectric sensors in the pneumatic industry and even the automation industry. Future research work includes further improving the lifetime of TLDS and encapsulating PMS to adapt it to different usage scenarios.

REFERENCES

- [1] M. De Volder, and D. Reynaerts, "Pneumatic and hydraulic microactuators: a review," *J. Micromech. Microeng.*, vol. 20, Mar. 2010, Art. no. 043001.
- [2] W. Li *et al.*, "Vibrational triboelectric nanogenerator-based multinode self-powered sensor network for machine fault detection," *IEEE/ASME Trans. Mechatronics.*, vol. 25, no. 5, pp. 2188–2196, Oct. 2020.
- [3] D. Gong, R. He, J. Yu, and G. Zuo, "A pneumatic tactile sensor for co-operative robots," *Sensors*, vol. 17, Nov. 2017, Art. no. 2592.
- [4] D. Stoianovici, A. Patriciu, D. Petrisor, D. Mazilu, and L. Kavoussi, "A new type of motor: pneumatic step motor," *IEEE/ASME Trans. Mechatronics.*, vol. 12, pp. 98–106, Feb. 2007.
- [5] M. Culjat, J. Franks, C. H. King, M. Franco, J. Bisley, W. Grundfest, and E. Dutson, "Pneumatic balloon actuators for tactile feedback in robotic surgery," *Ind. Rob.*, vol. 35, pp. 449–455, Aug. 2008.
- [6] L. Zhao, Y. Yang, Y. Xia, and Z. Liu, "Active disturbance rejection position control for a magnetic rodless pneumatic cylinder," *IEEE Trans. Ind. Electron.*, vol. 62, no. 9, pp. 5838–5846, Sep. 2015.
- [7] P. Ripka, A. Chirtsov, and V. Grim, "Contactless piston position transducer with axial excitation," *IEEE Trans. Magn.*, vol. 53, no. 11, Nov. 2017, Art. no. 4002504.
- [8] E. Hristoforou, P. D. Dimitropoulos, and J. Petrou, "A new position sensor based on the MDL technique," *Sens. Actuators A, Phys.*, vol. 132 no. 1, pp. 112–121, Nov. 2006.
- [9] S. Taghvaeeyan, R. Rajamani, and Z. Sun, "Non-Intrusive piston position measurement system using magnetic field measurements," *IEEE Sens. J.*, vol. 13, no. 8, pp. 3106–3114, Aug. 2013.
- [10] P. Ripka, M. Mirzaei, A. Chirtsov, and J. Vyhnanek, "Transformer position sensor for a pneumatic cylinder," *Sens. Actuators A, Phys.*, vol. 294, pp. 90–101, Aug. 2019.
- [11] F. R. Fan, Z. Q. Tian, and Z. L. Wang, "Flexible triboelectric generator," *Nano Energy*, vol. 1, no. 2, pp. 328–334, Mar. 2012.
- [12] S. Niu and Z. L. Wang, "Theoretical systems of triboelectric nanogenerators," *Nano Energy*, vol. 14, pp. 161–192, May. 2015.
- [13] Z. L. Wang, "On Maxwell's displacement current for energy and sensors: the origin of nanogenerators," *Mater. Today*, vol. 20, no. 2, pp. 74–82, Jan. 2017.
- [14] H. Yu *et al.*, "A self-powered dynamic displacement monitoring system based on triboelectric accelerometer," *Adv. Energy Mater.*, vol. 7, no. 19, Jun. 2017, Art. no. 1700565.
- [15] W. Yang, Y. Wang, Y. Li, J. Wang, T. Cheng, and Z. L. Wang, "Integrated flywheel and spiral spring triboelectric nanogenerator for improving energy harvesting of intermittent excitations/triggering," *Nano Energy*, vol. 66, Dec. 2019, Art. no. 104104.
- [16] K. Wang, J. Zhou, H. Ouyang, Y. Chang, and D. Xu, "A dual quasi-zero-stiffness sliding-mode triboelectric nanogenerator for harvesting ultralow-low frequency vibration energy," *Mech. Syst. Signal Process.*, vol. 151, Apr. 2021, Art. no. 107368.
- [17] X. Fu, *et al.*, "Breeze-wind-energy-powered autonomous wireless anemometer based on rolling contact-electrification," *ACS Energy Lett.*, vol. 6, no. 6, pp. 2343–2350, Jun. 2017.
- [18] H. Wang, J. Wang, X. Xia, D. Guan, and Y. Zi, "Multifunctional self-powered switch toward delay-characteristic sensors," *ACS Appl. Mater. Interfaces*, vol. 12, no. 20, pp. 22873–22880, May. 2020.
- [19] C. Rodrigues, *et al.*, "Emerging triboelectric nanogenerators for ocean wave energy harvesting: state of the art and future perspectives," *Energy Environ. Sci.*, vol. 13, no. 2, pp. 2657–2683, Jul. 2020.
- [20] C. Zhang, *et al.*, "Active resonance triboelectric nanogenerator for harvesting omnidirectional water-wave energy," *Joule*, vol. 5, no. 6, pp. 1613–1623, Jun. 2021.
- [21] H. Guo, *et al.*, "A highly efficient triboelectric negative air ion generator," *Nat. Sustain.*, vol. 4, pp. 147–153, Oct. 2020.
- [22] Y. Liu, B. Chen, W. Li, L. Zu, W. Tang, and Z. L. Wang, "Bioinspired triboelectric soft robot driven by mechanical energy," *Adv. Funct. Mater.*, vol. 31, no. 38, Sep. 2021, Art. no. 2104770.
- [23] T. Jin, *et al.*, "Triboelectric nanogenerator sensors for soft robotics aiming at digital twin applications," *Nat. Commun.*, vol. 11, no. 1, Oct. 2021, Art. no. 5381.
- [24] Z. Wang, *et al.*, "A self-powered angle sensor at nanoradian-resolution for robotic arms and personalized medicare," *Adv. Mater.*, vol. 32, no. 32, Aug. 2020, Art. no. 2001466.
- [25] Y. Xu, *et al.*, "Real-Time monitoring system of automobile driver status and intelligent fatigue warning based on triboelectric nanogenerator," *ACS Nano*, vol. 15, no. 4, pp. 7271–7278, Mar. 2021.

- [26] H. Zhang, Q. Cheng, X. Lu, W. Wang, Z. L. Wang, and C. Sun, "Detection of driving actions on steering wheel using triboelectric nanogenerator via machine learning," *Nano Energy*, vol. 79, Jan. 2021, Art. no. 105455.
- [27] Z. Wang, *et al.*, "Triboelectric flow sensor with float-cone structure for industrial pneumatic system monitoring," *Adv. Mater. Technol.*, vol. 4, no. 12, Dec. 2019, Art. no. 1900704.
- [28] Z. Wang, *et al.*, "Magnetic flap-type difunctional sensor for detecting pneumatic flow and liquid level based on triboelectric nanogenerator," *ACS Nano*, vol. 14, no. 5, pp. 5981–5987, Apr. 2020.
- [29] Q. Jing, Y. Xie, G Zhu, R. Han, and Z. L. Wang, "Self-powered thin-film motion vector sensor," *Nat. Commun.*, vol. 6, Aug. 2015, Art. no. 8031.
- [30] X. Zhang, Q. Gao, Q. Gao, X. Yu, T. Cheng, and Z. L. Wang, "Triboelectric rotary motion sensor for industrial-grade speed and angle monitoring," *Sensors*, vol. 21, Mar. 2021, Art. no. 1713.
- [31] W. Li, *et al.*, "Interdigitated electrode-based triboelectric sliding sensor for security monitoring," *Adv. Mater. Technol.*, vol. 3, no. 11, Aug. 2018, Art. no. 1800189.
- [32] Z. Xie, *et al.*, "Sweep-type triboelectric linear motion sensor with staggered electrode," *Extreme Mech. Lett.*, vol. 37, no. 10, Apr. 2020, Art. no. 100713.
- [33] S. Li, *et al.*, "A self-powered dual-type signal vector sensor for smart robotics and automatic vehicles," *Adv. Mater.*, vol. 34, no. 14, Apr. 2022, Art. no. 2110363.
- [34] S. Niu, *et al.*, "Theory of freestanding triboelectric-layer-based nanogenerators," *Nano Energy*, vol. 12, pp. 760–774, Mar. 2015.



Zitang Yuan was born in Shandong Province, China, in 1996. He received the B.S. degree in mechanical engineering from Qingdao University of Science and Technology, Qingdao, China, in 2020. He is currently studying for a M.S. degree in mechanical engineering at Changchun University of Technology. His research interests include pneumatic technology and triboelectric sensors.



Xiaosong Zhang was born in Sichuan Province, China, in 1996. He received the B.S. degree in mechanical engineering and automation from Changchun University of Technology, Changchun, China, in 2019, where he is currently working toward M.S. degree at the Department of Mechanical Engineering. His research interests include triboelectric nanogenerators, triboelectric sensors and piezoelectric actuators.



Qiang Gao was born in Shanxi Province, China, in 1994. He received the B.S. degree from the Luoyang Institute of Science and Technology, Luoyang, China, in 2018. He received M.S. in mechanical engineering at Changchun University of Technology, Changchun, China, in 2021. Now, he is studying in Beijing Institute of Nanoenergy and Nanosystems, Chinese Academy of Sciences, Beijing 101400, China. His research interests include friction drive mechanism and triboelectric nanogenerators, and intelligent mechanical sensing.



Zheng Wang was born in Jilin Province, China, in 1995. He received the M.S. degree in mechanical engineering from the Changchun University of Technology in 2021. Now he reads for the Ph.D. degree in Harbin Institute of Technology. And he is currently a visiting student at Beijing Institute of Nanoenergy and Nanosystems. His research interests are triboelectric nanogenerators and pneumatic technology.



Prof. Tinghai Cheng received the B.S. degree in mechanical design, manufacturing and automation, the M.S. degree in mechanical design and theory, and the Ph.D. degree in mechatronics engineering from the Harbin Institute of Technology, China, in 2006, 2008, and 2013, respectively. He was a visiting scholar in School of Materials Science and Engineering at Georgia Institute of Technology from 2017 to 2018. Currently, he is a professor of Beijing Institute of Nanoenergy and Nanosystems, Chinese Academy of Sciences and Changchun University of Technology. His research interests are piezoelectric actuators, piezoelectric energy harvester and triboelectric nanogenerators.



Prof. Zhong Lin Wang received his Ph.D. from Arizona State University in physics. He now is the Hightower Chair in Materials Science and Engineering, Regents' Professor, Engineering Distinguished Professor and Director, Center for Nanostructure Characterization, at Georgia Tech. Dr. Wang has made original and innovative contributions to the synthesis, discovery, characterization and understanding of fundamental physical properties of oxide nanobelts and nanowires, as well as applications of nanowires in energy sciences, electronics, optoelectronics and biological science. His discovery and breakthroughs in developing nanogenerators established the principle and technological road map for harvesting mechanical energy from environment and biological systems for powering personal electronics. His research on self-powered nanosystems has inspired the worldwide effort in academia and industry for studying energy for micro-nano-systems, which is now a distinct disciplinary in energy research and future sensor networks. He coined and pioneered the field of piezotronics and piezophotonics by introducing piezoelectric potential gated charge transport process in fabricating new electronic and optoelectronic devices. Details can be found at: <http://www.nanoscience.gatech.edu>.